Effect of external fields on low-frequency optical properties of achiral carbon tori

2010 J. Phys.: Condens. Matter 22 025302

(http://iopscience.iop.org/0953-8984/22/2/025302)

J. Phys.: Condens. Matter **22** (2010) 025302 (8pp) doi:10.1088/0953-8984/22/2/025302

Effect of external fields on low-frequency optical properties of achiral carbon tori

F L Shyu

Department of Physics, R.O.C Military Academy, Kaohsiung, Taiwan 830, Republic of China

E-mail: fl.shyu@msa.hinet.net

Received 13 October 2009, in final form 12 November 2009
Published 9 December 2009
Online at stacks.iop.org/JPhysCM/22/025302

Abstract

By using the tight-binding model including the curvature effect, the low-frequency electronic and optical properties with perpendicular polarization under electric and magnetic fields are studied for achiral carbon tori. Electronic properties (state energies, energy gaps, state degeneracy and wavefunctions) are strongly modulated by varying the direction and the magnitude of electric fields. The perpendicular magnetic field further enhances modulations of the electronic states. The variation of state energies and wavefunctions with external fields could be directly reflected in optical properties such as the amplitude and the frequency of absorption spectra and the exhibition of new peaks. Additionally, dependences of the low-frequency absorption peaks on electric fields, with and without magnetic fields, are significantly sensitive to the toroidal geometry.

1. Introduction

Since carbon nanotubes (CNs) were discovered in 1991 by Iijima [1], they have prompted a lot of studies because of their unique geometric structures and electronic properties. Carbon nanotubes, due to their nanoscaled size and diversified conductivity, have bright prospects in nanodevices. According to theoretical predictions, a single-walled carbon nanotube (SWNT) can be either metallic or semiconducting, and that this strongly depends on its geometric structure (diameter and/or chirality). The peculiar geometry-dependent electronic properties have been verified by scanning tunneling microscopy. When the two open ends of a carbon nanotube knit together seamlessly, a carbon toroid (CT) could be formed and was discovered by Liu *et al* [2].

From the scanning force microscopy image, a CT is a thin system which has a height or width of 1.0–1.2 nm and diameter of 300–500 nm. The new zero-dimensional system has attracted many investigations, such as electronic properties [3–10], magnetic properties [11–18], optical properties [19–21] and transport properties [22–24]. In experiments, low-temperature magnetotransport measurements on CTs have been performed, manifesting negative magnetoresistance and weak electron–electron interaction. They were predicted to be used to make interference devices [23]. Moreover, the small-sized CT as a transistor was used to measure current–voltage curves [25]. They revealed a sharp switching behavior, showing the possibility of nanoscaled electronic circuits composed of carbon tori. Recently, the temperature-dependent Raman spectra of CTs were studied [26]. It was found that the frequency decreases with increasing temperature for the radial-breathing mode and G-mode. In that sense, the result shows CTs have good thermal stability and thus have a large advantage for building new nanoscaled devices.

A carbon toroid can be constructed by cutting out a parallelogram from the graphite sheet, rolling it up into a nanotube by joining two opposite edges and then knitting together the open two ends of the nanotube. Therefore, the geometric structure of a CT could be described by two vectors specified in the unit cell of a CN. The first is a chiral vector $\mathbf{C_h} = m\mathbf{a}_1 + n\mathbf{a}_2$ in the circumferential direction and the second is the translational vector $\mathbf{T} = p\mathbf{a}_1 + q\mathbf{a}_2$ along the longitudinal direction. $\mathbf{a}_1$ and $\mathbf{a}_2$ are primitive lattice vectors of a graphite sheet. The parameters (m, n, p, q) uniquely define the geometric structure of a CT. The radius, height and chiral angle are, respectively, $R = b\sqrt{3(p^2 + pq + q^2)}/2\pi$, $2r = b\sqrt{3(m^2 + mn + n^2)}/\pi$ and $\theta = tan^{-1}[-\sqrt{3}n/(2m + n)]$. $b = 1.42$ Å is the C–C bond length. The achiral carbon tori include armchair carbon toroids (ACTs) and zigzag carbon toroids (ZCTs). An $(m, m, p, -p)$ armchair carbon toroid has $R = \sqrt{3}pb/2\pi$, $2r = 3mb/\pi$ and $\theta = -30°$. They are $R = 3pb/2\pi$, $2r = \sqrt{3}mb/\pi$ and $\theta = 0°$

for an $(m, 0, p, -2p)$ zigzag carbon toroid. $2r$ is also the diameter of the carbon nanotubes. Because of the periodic boundary conditions along the longitudinal and transverse directions, a CT presents discrete electronic states which are described by the transverse $(J = 1, 2, \ldots, N_u)$ and longitudinal $(L = 1, 2, \ldots, N_v)$ angular momenta. $N_u = (2/N_v)\sqrt{(m^2 + mn + n^3)(p^2 + pq + q^2)/3}$, and N_v is the double of the maximum common factor of (p, q). According to calculated energy gaps [3, 4], there are four types of carbon tori including the curvature effect: (I) $E_g \propto 1/r$, (II) $E_g \sim 0$ (ACTs), (III) $E_g \propto 1/R$ (ACTs) and (IV) $E_g \propto (1/r)^2$. The electronic structures (state energy, energy gap and state degeneracy) could be further affected by electric fields [7, 9, 10], magnetic fields [7–10], defects [7] and structural deformations [27].

For an electric field applied to carbon tori, the electrostatic potential energy obtained for each atom varies with the atomic position. The rotation symmetry of CTs should be destroyed. Therefore, the direction and the magnitude of electric fields will strongly affect the energy spectra [7, 9, 10]. While the electric field is small and parallel to the symmetric axis ($\mathbf{F}_\parallel$), electronic structures are hardly changed. However, the perpendicular electric field ($\mathbf{F}_\perp$), even for weak fields, drastically modulates the electronic states. It could induce state crossings that lead to a zero-gap transition ($E_g \neq 0 \rightarrow E_g = 0$). Moreover, the modulation of electronic states induced by the perpendicular electric fields has strong sensitivity to the toroidal geometry, i.e. it is very different for ACTs and ZCTs [10].

As a result of the cylindrical symmetry for CTs, as expected, the magnetic field will play an important role on the induced quantum effect such as Aharonov–Bohm oscillations. When carbon tori are threaded by a uniform magnetic field along the symmetric axis ($\mathbf{B}_\parallel$), the longitudinal angular momentum changes from L to $L + \phi/\phi_0$ (ϕ is magnetic flux and $\phi_0 = hc/e$). However, the perpendicular magnetic field $\mathbf{B}_\perp$ leads to the coupling of different Ls [8, 21]. According to theoretical studies, the effect of $\mathbf{B}_\perp$ on the energy gap is weaker than that of $\mathbf{B}_\parallel$. But the wavefunction interference induced by $\mathbf{B}_\perp$ will lead to peculiar oscillations of electric-field-dependent energy spectra [10]. Therefore, by adding electric and magnetic fields one may certainly induce interesting changes in the electronic properties of CTs.

The above-mentioned field-modulated energy spectra are expected to be directly reflected in optical properties. In particular, changes of absorption frequency with applied external fields could reveal modulations of external fields on energy dispersion. Also the height and number of absorption peaks could respectively show state degeneracy and changes of superposed wavefunctions. Besides, responses of optical properties to external fields also have a strong dependence on toroidal geometry. To study the remarkable band structure, the observation of optical spectra is one of the most useful experiments. In fact, microscopic structure or chirality of SWNTs was successfully identified by optical spectroscopies. Thus it is expected that optical measurements for CTs done as well as for SWNTs could verify the theoretical predictions in our study.

In this work, the $2p_z$ tight-binding model is used to investigate electronic states and optical spectra of achiral carbon tori in the presence of electric and magnetic fields. The curvature effect is included in the calculations. Electronic states are strongly affected by the direction and the magnitude of electric and magnetic fields. Moreover, the modulation of field-dependent electronic states also depends on toroidal geometry. Our study shows that there are significant differences in field-modulated electronic states between ACTs and ZCTs. Also, the geometry dependence of electronic states is fully reflected in optical properties.

2. Theory

The achiral CTs, chosen for a model study, include the $(m, m, p, -p)$ armchair carbon tori and $(m, 0, p, -2p)$ zigzag carbon tori. The π-electronic states are calculated from the nearest-neighbor tight-binding model with the curvature effect. There are $N = 4$ pm carbon atoms in each armchair or zigzag toroid. The Hermitian Hamiltonian matrix is built from the subspace spanned by the N wavefunctions of $2p_z$ orbitals. Under electric and magnetic fields, the nearest-neighbor Hamiltonian is given by

$$H = \sum_i \epsilon_i(\mathbf{F}) a_i^\dagger a_i - \sum_{i,j} t_{ij}(\mathbf{B}) a_i^\dagger a_j, \tag{1}$$

where $\epsilon_i(\mathbf{F})$ is the on-site energy due to the electric field and $t_{ij}(\mathbf{B})$ is the nearest-neighbor hopping integral associated with the magnetic field. $\{a_i^\dagger, a_j\}$ are creation and annihilation operators of fermions.

The $2p_z$ orbitals on the cylindrical and the toroidal surfaces are not parallel to one another, which induces the curvature effect. The curvature effect on the toroidal surface will be ignored because the toroidal diameter is much larger than the toroidal height. Thus the curvature effect on the cylindrical surface is only taken into account. It would lead to small fluctuations of the resonance integrals along different directions. At $\mathbf{B} = 0$, t_{ij}s based on different nearest-neighbor interactions are, respectively, given by $\gamma_1 = \gamma_0(1 - b^2 \sin^2\theta/8r^2)$, $\gamma_2 = \gamma_0[1 - b^2(\sin\theta + \sqrt{3}\cos\theta)^2/32r^2]$ and $\gamma_3 = \gamma_0[1 - b^2(\sin\theta - \sqrt{3}\cos\theta)^2/32r^2]$. γ_0 ($\sim$3 eV) is the resonance integral without the curvature effect [3, 4].

For carbon nanotubes, the optical absorption spectra excited by an EM field with perpendicular polarization were studied by Ajiki and Ando [30]. Their studies showed that the depolarization effect due to the charge screening could strongly suppress optical absorption spectra. Hence, electric fields ($\mathbf{F}$) in equation (1) are regarded as effective fields that might be relatively suitable. When an electric field is applied to CTs, the electric potential will change the on-site energy. The effective electric field is assumed to be $\mathbf{F} = F\cos\alpha_F \hat{Z} + F\sin\alpha_F \hat{X} = \mathbf{F}_\parallel + \mathbf{F}_\perp$, where α_F is the angle between $\mathbf{F}$ and the symmetric axis ($\hat{Z}$). The unit of F is γ_0 Å^{-1} here and henceforth. We use the rectangular coordinates (X, Y, Z) for convenience, and choose the center of the toroid as the origin. The coordinates (x_i, y_i) of the ith atom in a graphite plane are transferred to (X_i, Y_i, Z_i). Such coordinates are further expressed as

$X_i = \rho_i \cos\Omega$, $Y_i = \rho_i \sin\Omega$ and $Z_i = r \sin\beta$. ρ_i is the perpendicular distance between the ith atom and the symmetric axis. $\Omega = y_i/R$ and $\beta = x_i/r$ are azimuthal angles of carbon toroids and carbon nanotubes, respectively. Due to the electric field, the diagonal elements of the Hamiltonian matrix are changed from zero to

$$H_{ii} = -F \cos\alpha_F Z_i - F \sin\alpha_F X_i. \tag{2}$$

Also it is noticed that applied electric fields with any direction will destroy rotational symmetry of CTs, hence the transverse and the longitudinal momenta are no longer good quantum numbers. The wavefunction could be conveniently expanded in real space according to all the 4 pm $2p_z$ orbitals.

Moreover, the hopping parameter could be further modified by the Peierls phase (G_{ij}) which is induced by the applied magnetic field [8, 17]. The magnetic field is assumed to be $\mathbf{B} = B\cos\alpha_B \hat{Z} + B\sin\alpha_B \hat{R} = \mathbf{B}_\parallel + \mathbf{B}_\perp$. α_B is the angle between $\mathbf{B}$ and the symmetric axis. The cylindrical coordinates (R, Ω, Z) are used for simplicity. The vector potential is chosen to be $\mathbf{A} = RB\cos\alpha_B/2\hat{\Omega} + RB\sin\alpha_B \sin\Omega\hat{Z}$. It causes the magnetic phase factor $G = \int \mathbf{A}\cdot d\mathbf{R}$. Therefore, the hopping parameter t_{ij} would be changed to $t_{ij}e^{iG_{ij}}$. State energies of achiral carbon tori could be obtained by diagonalizing the 4 pm × 4 pm Hamiltonian matrix. They could be expressed as $E^{c,v}(\mathbf{F}, \mathbf{B})$. c and v, respectively, correspond to unoccupied and occupied states.

In order to study low-frequency optical properties, a CT is assumed to be excited by the EM field. The electric polarization ($\hat{e}_p$) is considered to be perpendicular to the symmetric axis. At zero temperature, electrons are excited from the occupied π states to the unoccupied $\pi^\star$ states. The low-frequency spectral function from the Fermi golden rule is given by

$$A(\omega) \propto \frac{1}{m_e^2} \sum_{h',h;l',l} |\langle \Phi^{h'}(l')|\hat{e}_p \cdot \nabla|\Phi^h(l)\rangle|^2 \times \mathrm{Im}\left\{\frac{f(E^{h'}) - f(E^h)}{E_{l'}^{h'} - E_l^h - \omega + i\Gamma}\right\}, \tag{3}$$

where $\Phi^{h'}(l')$ and $\Phi^h(l)$ ($E_{l'}^{h'}$ and E_l^h) are the wavefunctions (state energies) of the final and initial states. h (h') represents v or c and l (l') is denoted as the subband index. $\Gamma = 5\times10^{-4}\,\gamma_0$ is the energy width due to various de-excitation mechanisms and $f(E^h)$ is the Fermi–Dirac distribution function. Here, $\langle \Phi^{h'}(l')|\hat{e}_p \cdot \nabla|\Phi^h(l)\rangle = \hat{e}_p \cdot \mathbf{D}_{l'l}^{h'h}$ is the dipole matrix element [28, 29], which is the inner product of the electric polarization $\hat{e}_p$ and the dipole vector $\mathbf{D}_{l'l}^{h'h}$. Obviously, the calculated spectral function is determined by the number of effective transition channels and the dipole vector along the electric polarization. By the tight-binding model, the wavefunctions of final and initial states in real space could be expanded by individual atomic eigenfunctions, i.e. $|\Phi^{h'}(l')\rangle = \sum_i a_i^{h'l'}|\phi_i\rangle$ and $|\Phi^h(l)\rangle = \sum_j b_j^{hl}|\phi_j\rangle$. The dipole vector could be simply written as

$$\mathbf{D}_{l'l}^{h'h} = M \sum_{i,j} a_i^{h'l'\star} \hat{u}_{ij} b_j^{hl}, \tag{4}$$

where M is the optical matrix element for two nearest-neighbor atoms, which is well defined and used to calculate the optical properties of the graphite sheet and the CNs [28, 29]. $\hat{u}_{ij}$ is the unit vector from site i to site j.

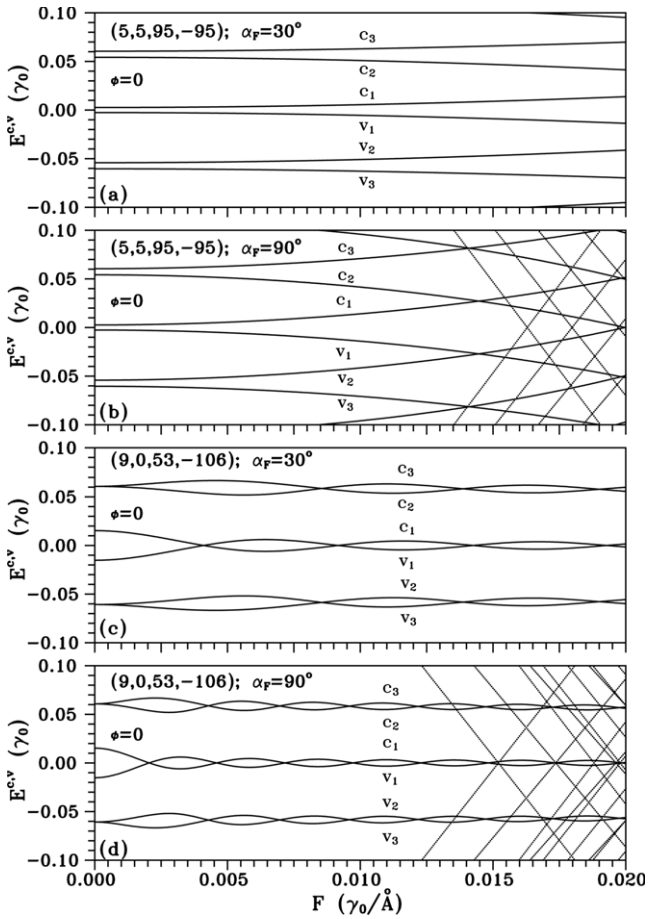

Figure 1. F-dependent low energy electronic states at $\phi = 0$ and (a) $\alpha_F = 30°$ and (b) $\alpha_F = 90°$ for the (5, 5, 95, −95) CT; (c) $\alpha_F = 30°$ and (d) $\alpha_F = 90°$ for the (9, 0, 53, −106) CT.

3. Results and discussions

For achiral CTs, the (5, 5, 95, −95) ACT and the (9, 0, 53, −106) ZCT are mainly considered geometric structures. They have the same height ($2r = 6.8$ Å) and their radii are nearly equal to 36 Å. In order to understand the field-modulated electronic properties, the electronic states of CTs in the absence of external fields are simply reviewed. Their occupied and unoccupied states are symmetric to the Fermi level ($E_F = 0$). CTs might have an energy gap between the highest occupied molecular orbital (HOMO) and the lowest unoccupied molecular orbital (LUMO). For example, figures 1(a) and (c) show that energy gaps at $\mathbf{F} = 0$ are $E_g = 0.0052\ \gamma_0$ and $E_g = 0.0304\ \gamma_0$ for the (5, 5, 95, −95) and the (9,0,53,-106) CTs, respectively. The electronic states of ACTs have double degeneracy with the relation $E(J, L) = E(J, N_v - L)$, e.g. $E(5, 32) = E(5, 158)$ for the HOMO and LUMO states of the (5, 5, 95, −95) CT. But ZCTs with higher symmetry could exhibit fourfold degenerate states except for doubly degenerate HOMO and LUMO states. The fourfold and double degeneracies, respectively, come from $E(J, L) =$

$E(J, N_v - L) = E(N_u - J, N_v/2 - L) = E(N_u - J, N_v/2 + L)$ and $E(J_a, L_a) = E(N_u - J_a, L_a + N_v/2)$ [3]. (J_a, L_a) represents the state nearest to the Fermi level. For the $(9, 0, 53, -106)$ CT, (J_a, L_a) state is a (3, 53) or (6, 106) state. State energy and state degeneracy could be changed by applied external fields and thus directly reflected in optical properties.

First we make a detailed study of the low energy electronic states at $\mathbf{F} \neq 0$ and $\mathbf{B} = 0$. While the applied electric field is $F = 0.02\ \gamma_0$ Å^{-1}, the electric potential difference of CTs along the symmetric axis is about 0.4 V. The on-site energy $\epsilon_i(\mathbf{F}_\parallel)$, at $\alpha_F = 0°$, is much smaller than the typical hopping integral γ_0 such that electronic structures are hardly changed. State energies are gradually affected with increasing electric field, e.g. $F > 0.05\ \gamma_0$ Å^{-1}. From the perturbation point of view, $\mathbf{F}_\parallel$ leads to the coupling of wavefunctions with different Js at $\mathbf{F} = 0$. At the large $\mathbf{F}_\parallel$, the strong coupling has a significant effect on electronic properties such as state energy, state degeneracy, energy gap and wavefunction (not shown here). However, the state symmetry about $E_F = 0$ is not broken by $\mathbf{F}_\parallel$. This result remains unchanged even for other electric and magnetic fields.

While the electric field deviates from the symmetric axis, the electric potential difference along the toroidal diameter is much larger than that along the symmetric axis. Then its perpendicular component ($\mathbf{F}_\perp$) starts affecting significantly state energies. It could be seen in figure 1(a) for the $(5, 5, 95, -95)$ CT at $\alpha_F = 30°$. The calculated result reveals that state energies gradually increase (c_1, c_3 and v_2 subbands) or decrease (c_2, v_1 and v_3 subbands) with the increasing $\mathbf{F}_\perp$, whereas the state degeneracy is unchanged. v_n (c_m) denotes the $n(m)$th valence (conduction) subband from the Fermi level. While the field direction is much closer to the toroidal surface, e.g. $\alpha_F = 90°$, electronic states are apparently modulated even for the weak field, as shown in figure 1(b). State energies would drastically become large or small with the increasing $\mathbf{F}_\perp$ that leads to state crossings. Especially at large $\mathbf{F}_\perp$, such state crossings happen more frequently. State crossings would cause the energy gap to vanish at certain electric fields. Additionally, field-dependent state energies appear linearly dispersed at $F > 0.0135\ \gamma_0$ Å^{-1}. More electronic states are shifted into the low and extreme energy regions. Thus electronic states at large electric fields are denser than those at weak electric fields, i.e. there are more transition channels. Except for the modulation of state energies, $\mathbf{F}_\perp$ also changes state degeneracy. The electronic states corresponding to crossing points and linear dispersion would exhibit fourfold degeneracy, the others remaining doubly degenerate. However, the state degeneracy will be destroyed again at larger $\mathbf{F}_\perp$, e.g. a lot of singlet states exist at $F_\perp = 0.05\ \gamma_0$ Å^{-1} [10]. These results could be explained as follows: $\mathbf{F}_\perp$ would break the circumferential symmetry, thus making the different isolated L states (at zero field) superposed. The coupling strength, at large $\mathbf{F}_\perp$, is different between $|J, L + m\rangle$ and $|J, L - m\rangle$ states that causes the destruction of state degeneracy [10]. Thus the effects of $\mathbf{F}_\perp$ on electronic structures are much stronger than those of $\mathbf{F}_\parallel$, and clearly reflect the geometric feature, i.e. the radius is much larger than the height. As compared with the $(5, 5, 95, -95)$ ACT, figures 1(c) and (d) show the modulation of electronic states induced by $\mathbf{F}_\perp$ is stronger for the $(9, 0, 53, -106)$ ZCT. There are more state crossings, and the energy gap vanishes at the smaller electric fields with increasing α_F. It makes the zero-gap transition happen more frequently. The large $\mathbf{F}_\perp$ also makes a lot of linear dispersion states group together. Moreover, fourfold degeneracy (at $\mathbf{F}_\perp = 0$) are changed into double degeneracy. Except for crossing points with fourfold degeneracy, the other electronic states, including linear dispersion, are all doubly degenerate.

The above-mentioned $\mathbf{F}_\perp$-modulated electronic properties could be further validated by absorption spectra. The frequency of absorption spectra is determined by energy spacing. Numbers and heights of absorption peaks are dependent on numbers of effective transition channels and the component of the dipole matrix element along the polarization direction of incident light. Based on the selection rule of optical transitions at $\mathbf{F} = 0$, excitation from the initial state $|J, L\rangle$ to the final state $|J', L'\rangle$ must satisfy ($\Delta J = \pm 1$, $\Delta L = 0$) for polarization along the symmetric axis and ($\Delta J = 0$, $\Delta L = \pm 1$) for polarization perpendicular to the symmetric axis, respectively. The differences of state energy for various Js electronic states are large. Therefore, low-frequency absorption spectra induced by the perpendicular polarization are mainly studied by the selection rule ($\Delta J = 0$, $\Delta L = \pm 1$). Additionally, due to the symmetry of state energies about $E_F = 0$, the optical transition from the v_n subband to the c_m subband simultaneously accompanies another transition $v_m \rightarrow c_n$. Figure 3(a) shows the low-frequency absorption spectra for $F = 0$ and $F \neq 0$ ($F = 0.01$ and $0.02\ \gamma_0$ Å^{-1}) at $\alpha_F = 30°$. In the absence of electric fields, the highest peak ($\omega = 0.056\,75\gamma_0$, $A = 0.8$) comes from the transition $v_1 \rightarrow c_2$ ($|5, 32\rangle$ state $\rightarrow$ $|5, 31\rangle$ state) and the second peak ($\omega = 0.063\ \gamma_0$, $A = 0.02$) with a very weak dipole matrix element is due to the transition $v_1 \rightarrow c_3$ ($|5, 32\rangle$ state $\rightarrow$ $|5, 33\rangle$ state). At $\alpha_F = 30°$, $F = 0.01\ \gamma_0$ Å^{-1} hardly changes the absorption spectra of $F = 0$. At the larger electric field, $F = 0.02\ \gamma_0$ Å^{-1}, the changes in energy spacing and coupling of different Ls states are obvious. Thus the shift of absorption frequency and induced new peaks could be observed. The two new absorption peaks around $\omega \approx 0.11\gamma_0$ are due to the transitions $v_1 \rightarrow c_4$ and $v_2 \rightarrow c_3$. As α_F increases, e.g. $\alpha_F = 90°$, the larger $\mathbf{F}_\perp$ modulates energy spacing that causes a shift of absorption peaks. Moreover, the coupling effect of different Ls states are greatly enhanced such that at higher energy levels the components with larger angular momenta gradually grow. That would lead to an increase in numbers of transition channels. In other words, the height and the number of new peaks thus increase, whereas the first peak height is reduced, as shown in figure 3(b). Also noticed is that, though more linear subbands are induced by $\mathbf{F}_\perp$, they could not exhibit effective transition channels resulting in no contribution to absorption spectra. As to the $(9, 0, 53, -106)$ ZCT, the most prominent peak at $F = 0$, in figure 3(c), comes from transitions of doubly degenerate states to fourfold degenerate states. As compared with an ACT, though a ZCT has more transition channels, the weaker dipole matrix element leads to the lower absorption peak. According to figures 3(c) and (d), the differences of $\mathbf{F}$-modulated absorption spectra between an

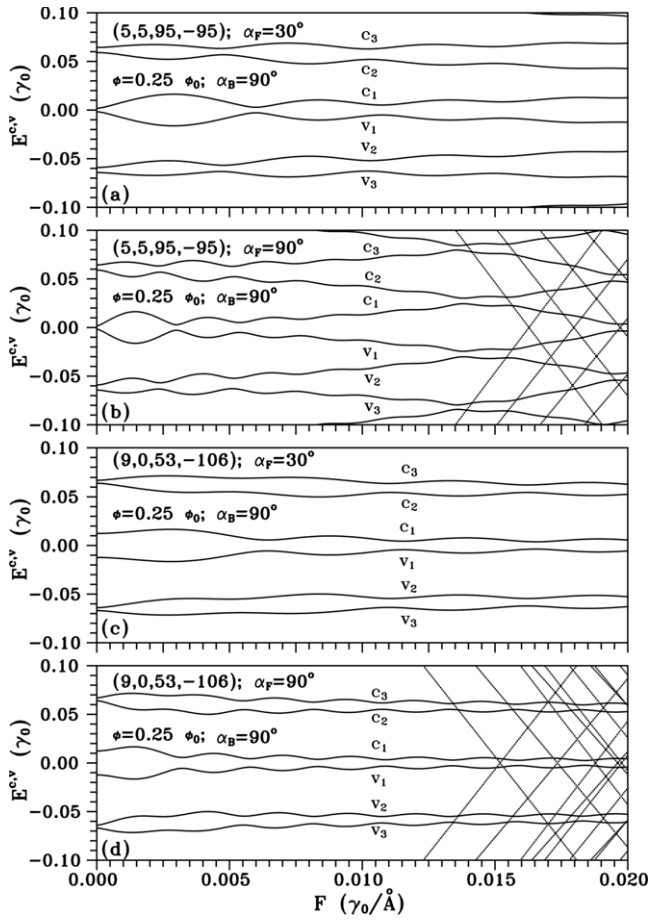

Figure 2. Similar plot as figure 1, but shown for $\phi = 0.25\phi_0$ and $\alpha_B = 90°$.

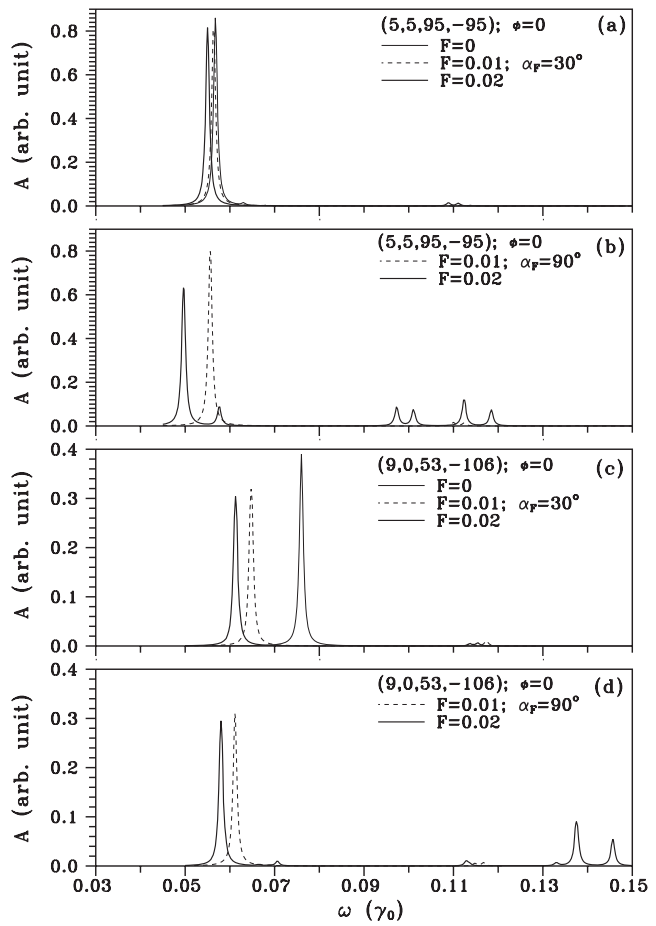

Figure 3. Absorption spectra for different Fs are calculated at $\phi = 0$ and (a) $\alpha_F = 30°$ and (b) $\alpha_F = 90°$ for the $(5, 5, 95, -95)$ CT; (c) $\alpha_F = 30°$ and (d) $\alpha_F = 90°$ for the $(9, 0, 53, -106)$ CT.

ACT and a ZCT could be described as follows: (I) a shift of absorption frequency is more obvious between $F = 0$ and $F \neq 0$ for the latter and (II) new absorption peaks induced by $\mathbf{F}_\perp$ are fewer and those happen at higher frequency for the latter. These calculated results demonstrate that **F**-modulated low-frequency electronic and optical properties have strong geometry dependence.

In addition to electric fields, electronic states of carbon tori are further changed by the magnetic field. For the applied magnetic flux $\phi = 0.25\phi_0$, it corresponds to a magnetic field of the order of 25 T. The main effect of the parallel magnetic field ($\mathbf{B}_\parallel$) is to change L into $L + \phi/\phi_0$. Thus the doubly degenerate states are broken into two singlet states by $\mathbf{B}_\parallel$. The more increasing and decreasing states would lead to more state crossings (not shown here). The zero-gap transition would occur at the smaller electric fields [10]. As compared with $\mathbf{B}_\parallel$, $\mathbf{B}_\perp$ has weaker effects on changing state energies. Its main effect is to cause the superposition of different Ls electronic states. As a result of electronic state interference induced by magnetic phase, state energies obviously oscillate with increasing electric fields. It could be seen in figure 2(a) for the $(5, 5, 95, -95)$ ACT at $\alpha_F = 30°$; $\phi = 0.25\phi_0$ and $\alpha_B = 90°$. As α_F increases, e.g. $\alpha_F = 90°$, figure 2(b) shows that the oscillation of state energy is more frequent and some state crossings open at larger electric fields. Moreover, the amplitudes of oscillations are reduced with increasing electric fields. Also the linearity of state energies at large electric fields is not destroyed. The large electric fields dominating the coupling effect and $\mathbf{B}_\perp$ not destroying state degeneracy are the main reasons. As to the ZCT, figures 2(c) and (d) show that effect-induced $\mathbf{B}_\perp$ are similar to those for the ACT. However, at $F = 0$, the fourfold degenerate states are reduced to doubly degenerate states. It is noted that, for the $(m, m, p, -p)$ ACTS, whether the state crossing opening happens at smaller $\mathbf{F}_\perp$ is determined by its geometric structure, i.e. the modulo of p with respect to 3. But it is not true for the ZCTs as shown in [24].

The modulation of **F**-dependent state energies induced by $\mathbf{B}_\perp$ is directly reflected in absorption spectra as shown in figure 4. For the ACT, the coupling effect of different Ls states induced by $\mathbf{B}_\perp$ would exhibit new absorption peaks. Comparisons among figures 3(a), (b), 4(a) and (b) show that the first low-frequency peak at $\mathbf{B}_\perp = 0$ will split into two lower peaks. Then the differences of absorption frequency for the first two peaks clearly depend on the magnitude of electric fields. Besides, extra lower absorption peaks emerge at high frequency. These results mainly come from competition of the coupling effect of different Ls states induced by $\mathbf{F}_\perp$ and $\mathbf{B}_\perp$. Notice that the peak height of the second peak is higher than

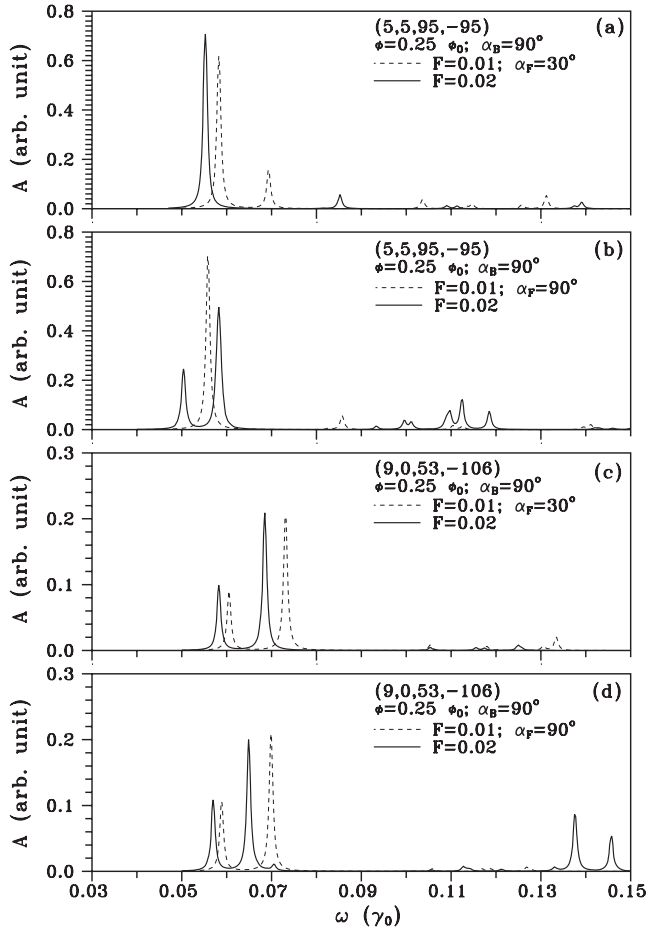

Figure 4. Similar plot as figure 3, but shown for $\phi = 0.25\phi_0$ and $\alpha_B = 90°$.

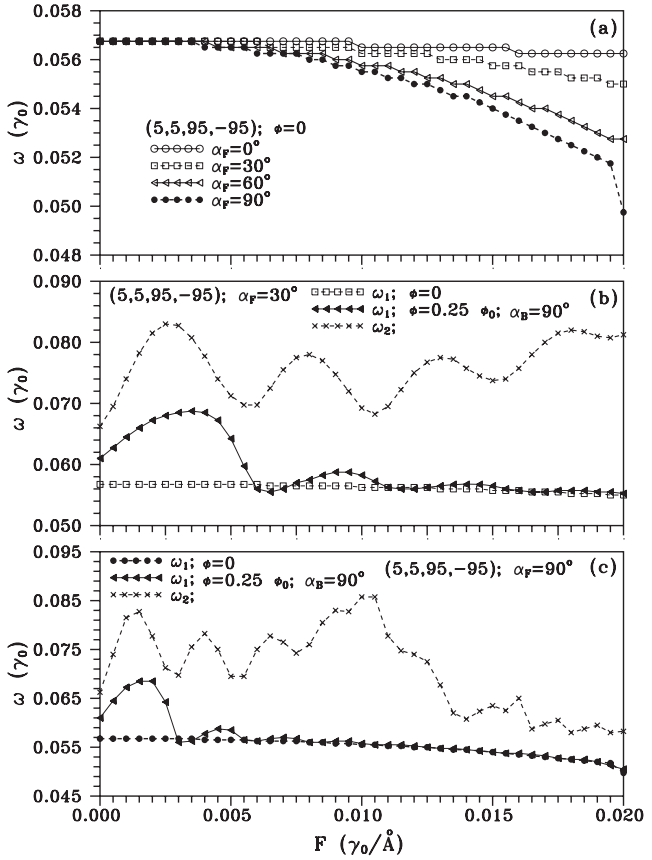

Figure 5. Low energy absorption frequency of the (5, 5, 95, −95) CT at (a) $\phi = 0$ and different α_Fs, (b) $\alpha_F = 30°$, $\phi = 0.25\phi_0$ and $\alpha_B = 90°$, and (c) $\alpha_F = 90°$, $\phi = 0.25\phi_0$ and $\alpha_B = 90°$. In (b) and (c), those at $\phi = 0$ are also shown for comparison. The solid (dashed) lines are drawn as indications.

that of the first peak as shown in figure 4(b). It demonstrates that $\mathbf{B}_\perp$, at larger $\mathbf{F}_\perp$, could strongly enhance the coupling effect for energy levels that are closer to the Fermi energy. As to the ZCT, figures 4(c) and (d) show that effects of $\mathbf{B}_\perp$ on absorption spectra are similar to those for the ACT. But there exist some differences for the ZCT; they include (I) the coupling effect induced by $\mathbf{B}_\perp$ is also evident even for smaller $\mathbf{F}_\perp$ and (II) the frequency differences between the first two peaks are almost the same as α_F increases. This shows that the coupling effects induced by $\mathbf{B}_\perp$ are strongly dependent on toroidal geometry.

From figure 3, it is obvious that the first low-frequency absorption peak due to the larger transition probability presents the largest peak height. In that sense, it is more easily observed as the threshold excitation energy in experiments. Therefore, it deserves to be investigated as the **F**-dependent absorption frequency of the first peak for different α_Fs. For the ACT, the lowest-frequency peak mainly comes from the transition $v_1 \rightarrow c_2$. Figure 5(a) shows that ω at $\alpha_F = 0°$ is nearly unchanged with increasing F. As α_F increases, ω gradually decreases. A decrease in ω with increasing F is getting faster as α_F grows. The maximum difference of excitation frequency is $\Delta\omega_{\max} = 0.007\ \gamma_0$ while the magnitude of applied electric fields changes from $F = 0$ to $0.02\ \gamma_0$ Å^{-1}. These results reveal the characteristic of **F**-modulated state energies from dispersionless to parabolic dispersion with increasing α_F. However, for the ZCT, ω drastically oscillates with increasing electric fields except for $\alpha_F = 0°$, as shown in figure 6(a). The oscillating amplitude and period decrease as α_F grows. Moreover, the maximum difference of excitation frequency is $\Delta\omega_{\max} = 0.018\ \gamma_0$, much larger than that for the ACT. Relatively, it is easily observed in experiments for the ZCT. From the above, it is very evident that the **F**-modulated energy dispersion and low energy absorption frequency have strong geometry dependence.

The quantum effects induced by applied magnetic fields on absorption spectra are further investigated. Except for enhancing the oscillation of F-dependent state energy, the other important effect of $\mathbf{B}_\perp$ is to alter the probability of different L components in the wavefunction. That leads to a change in transition channels and thus induces new absorption peaks. It could be validated by calculating **F**-dependent absorption frequencies of the first two peaks at $\phi = 0.25\phi_0$ and $\alpha_B = 90°$. For the ACT, at $\alpha_F = 30°$, ω_1 (ω_2) denotes the absorption frequency of the first (second) peak for the lower (higher) energy, as shown in figure 5(b). At $F = 0$, $\mathbf{B}_\perp$ induces a new transition channel $v_1 \rightarrow c_3$ except for the channel $v_1 \rightarrow c_2$ at $\mathbf{B}_\perp = 0$. ω_1 ($v_1 \rightarrow c_2$) significantly oscillates at small

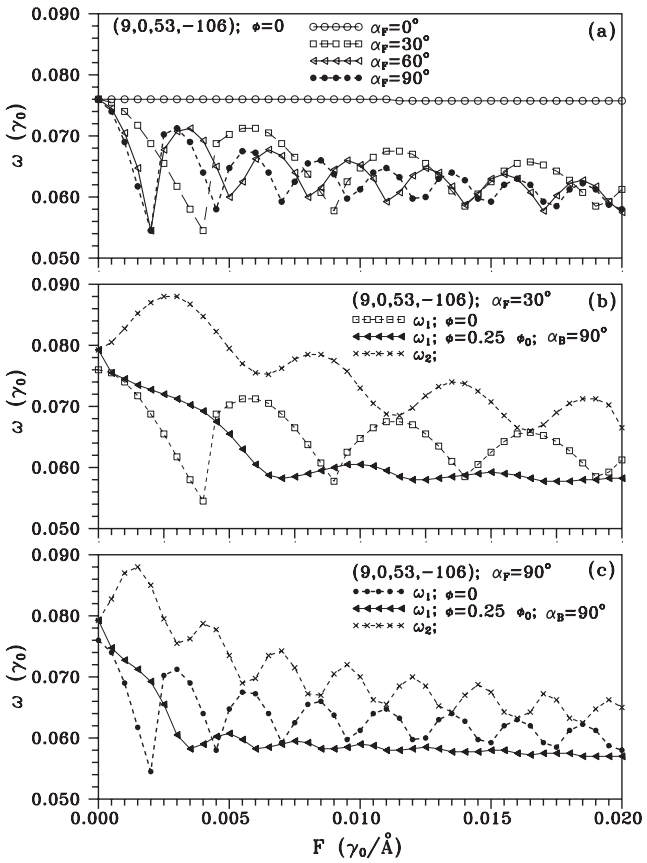

Figure 6. Similar plot as figure 5, but shown for the (9, 0, 53, −106) CT.

F but the oscillation, at $F > 0.01\ \gamma_0$ Å^{-1}, almost vanishes and ω_1 approaches the case of $\phi = 0$. The main reason is the energy spacing between v_1 and c_2 subbands is hardly changed by $\mathbf{B}_\perp$ at large electric fields. As compared with ω_1, the F dependence of ω_2 presents very different behavior. As F increases, ω_2 keeps oscillating and its magnitude gradually grows. The reason is that coupling effects induced by both $\mathbf{F}_\perp$ and $\mathbf{B}_\perp$ are enhanced by increasing F. Thus the higher energy transition channel such as $v_2 \rightarrow c_2$ is exhibited. While α_F increases to $\alpha_F = 90°$, the larger perpendicular component of $\mathbf{F}$ will fully dominate the modulation of energy dispersion. With a comparison between figures 5(b) and (c), we can see F-dependent ω_1 at $\alpha_F = 90°$ approaches the case of $\phi_0 = 0$ at smaller F. It reveals that the effect of $\mathbf{F}_\perp$ on the lower-frequency absorption spectra becomes stronger than $\mathbf{B}_\perp$. As to ω_2, figure 5(c) shows a complicated $\mathbf{F}_\perp$ dependence. The larger $\mathbf{F}_\perp$ strongly enhances the coupling effect of different L states and then induces new transition channels. Thus ω_2, at $F > 0.009\ \gamma_0$ Å^{-1}, oscillates irregularly with increasing F. The complicated oscillation results from the competition between $v_1 \rightarrow c_3$ and $v_2 \rightarrow c_2$ transition channels.

Furthermore, comparisons among figures 5(b), (c), 6(b) and (c) show that the F dependence of absorption frequency under $\mathbf{B}_\perp$ is also sensitive to the toroidal geometry. For the ZCT, figures 6(b) and (c) show that only one absorption frequency exists at $F = 0$ because $\mathbf{B}_\perp$ does not induce new transition channels. For the first peak, ω_1 with increasing F quickly decreases at small F and then oscillates. The oscillating amplitude is gradually reduced with increasing F, especially for $\alpha_F = 90°$. It shows that the F dependence of ω_1 is weaker at larger α_F. The main reason is that $\mathbf{B}_\perp$ strongly suppresses the change in energy spacing between the v_1 and c_3 subbands. As to ω_2, its F dependence shows a regular oscillation that is similar to the case of $\phi = 0$, except at small F. In the ZCT, the oscillatory behavior of ω_2 is more regular than that in the ACT (in figure 5(d)). As F increases, the transition channel of ω_2 from the v_1 subband to the c_3 subband is the main cause. From the above, the external field dependences of ω_1 and ω_2 have great sensitivity to toroidal geometry. It is expected to be identified by experiments.

4. Conclusion

In this work, we have used the tight-binding model with curvature effect to study the low-frequency electronic and optical properties of achiral carbon tori in the presence of electric and magnetic fields. The studied results show that modulations of electronic states have strong dependence on the direction and the magnitude of electric fields and geometric structure (chiral angle). $\mathbf{F}_\perp$ leads to the state crossing, zero-gap transition and the destruction of state degeneracy. Moreover, it breaks the circumferential symmetry of CTs that makes different L states at the $F = 0$ coupling. With increasing $\mathbf{F}_\perp$, the growing coupling effect results in the exhibition of more new transition channels. Such changes in electronic states are further enhanced by $\mathbf{B}_\perp$ and are directly reflected in optical properties; they include (I) alterations in positions and amplitudes of absorption peaks, and (II) the exhibition of new peaks. Due to the competition between $\mathbf{F}_\perp$ and $\mathbf{B}_\perp$ in coupling effects, ωs corresponding to the first two peaks present very distinct oscillatory behaviors with increasing F. These remarkable results have strong dependence on toroidal geometry. The predicted low-frequency electronic and optical properties in external fields could be verified by optical measurements.

Acknowledgments

The author would like to thank the National Center for High-Performance Computing. This work was supported in part by the National Science Council of Taiwan, Republic of China under grant no. NSC 98-2112-M-145-003-MY3.

References

[1] Iijima S 1991 *Nature* **354** 56
[2] Liu J, Dai H, Hafner J H, Colbert D T, Smalley R E, Tans S J and Dekker C 1997 *Nature* **385** 780
[3] Lin M F, Chen R B and Shyu F L 1998 *Solid State Commun.* **107** 227
[4] Lin M F and Chuu D S 1998 *J. Phys. Soc. Japan* **67** 259
[5] Oh D H, Park J M and Kim K S 2000 *Phys. Rev.* B **62** 1600
[6] Ceulemans A, Chibotaru L F and Bovin S A 2000 *J. Chem. Phys.* **112** 4271

[7] Latgé A, Rocha C G, Wanderley L A L, Pacheco M, Orellana P and Barticevic Z 2003 *Phys. Rev.* B **67** 155413
[8] Shyu F L, Tsai C C, Chang C P, Chen R B and Lin M F 2004 *Carbon* **42** 2879
[9] Rocha C G, Pacheco M, Barticevic Z and Latgé A 2004 *Phys. Rev.* B **70** 233402
[10] Shyu F L, Tsai C C, Lin M F and Hwang C C 2006 *J. Phys. Soc. Japan* **75** 104710
[11] Meunier V, Lambin P and Lucas A A 1998 *Phys. Rev.* B **57** 14886
[12] Haddon R C 1997 *Nature* **388** 31
[13] Lin M F 1998 *J. Phys. Soc. Japan* **67** 1094
[14] Lin M F and Chuu D S 1998 *Phys. Rev.* B **57** 6731
[15] Liu L, Guo G Y, Jayanthi C S and Wu S Y 2002 *Phys. Rev. Lett.* **88** 217206
[16] Latil S, Roche S and Rubio A 2003 *Phys. Rev.* B **67** 165420
[17] Tsai C C, Shyu F L, Chiu C W, Chang C P, Chen R B and Lin M F 2004 *Phys. Rev.* B **70** 075411
[18] Shyu F L 2009 *Physica* E **41** 537
[19] Lin M F 1998 *Phys. Rev.* B **58** 3629
[20] Lin M F 1998 *J. Phys. Soc. Japan* **62** 2218
[21] Shyu F L 2005 *Phys. Rev.* B **72** 045424
[22] Lin M F 1999 *J. Phys. Soc. Japan* **68** 3744
[23] Shea H R, Martel R and Avouris P 2000 *Phys. Rev. Lett.* **84** 4441
[24] Shyu F L 2008 *Solid State Commun.* **148** 485
[25] Watanabe H, Manabe C, Shigematsu T and Shimizu M 2001 *Appl. Phys. Lett.* **78** 2928
[26] Song L, Ma W, Ren Y, Zhou W, Xie S, Tan P and Sun L 2008 *Appl. Phys. Lett.* **92** 121905
[27] Zhang Z, Yang Z, Wang X, Yuan J, Zhang H, Qiu M and Peng J 2005 *J. Phys.: Condens. Matter* **17** 4111
[28] Saito R, Grüneis A, Samsonidze G G, Dresselhaus G, Dresselhaus M S, Jorio A, Cançado L G, Pimenta M A and Souza Filho M A 2004 *Appl. Phys.* A **78** 1099
[29] Jiang J, Saito R, Grüneis A, Dresselhaus G and Dresselhaus M S 2004 *Carbon* **42** 3169
[30] Ajiki H and Ando T 1994 *Physica* B **201** 349